Supporting Information

From Toxic Pollutant to Catalyst: One-Pot Synthesis of Fe_3O_4-Ni-DBP/NF for Efficient Overall Water Splitting

Qingyuan Song [a, b], Jinshou Yao [a], Liujun Jin [a, *], Peiyang Gu [a], Ye Wang [c], Ping Liu [a, *], Congping Chen [c], Guohong Dai [c, d*]

[a] *School of Petrochemical Engineering, Changzhou University, Changzhou, 213164, PR China*

[b] *School of Safety Science and Engineering, Changzhou University, Changzhou, 213164, Jiangsu, PR China*

[c] *School of Mechanical Engineering and Rail Transit, Changzhou University, Changzhou, 213164, Jiangsu, PR China*

[d] *School of Mechanical Engineering, Jiangsu University of Technology, Changzhou, 213164, Jiangsu, PR China*

E-mail: jinlj@cczu.edu.cn, pingliu@cczu.edu.cn, dgh@cczu.edu.cn

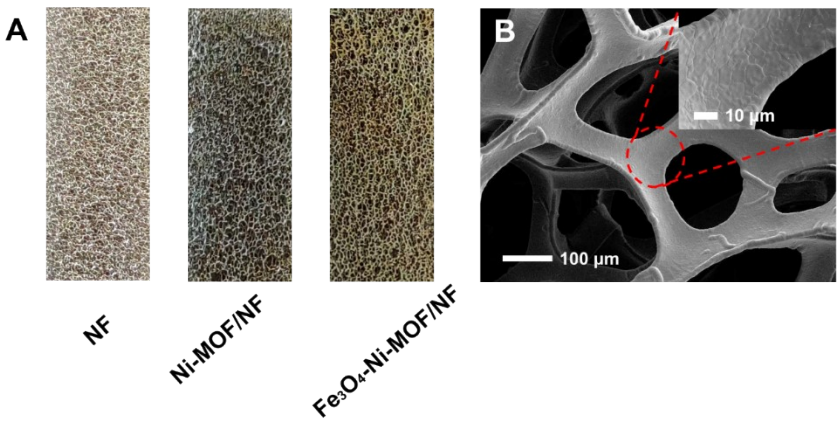

Figure S1. (A) Color changes in the appearance of the NF, Ni-DBP, and Fe_3O_4-Ni-DBP. (B) FE-SEM image of bare NF.

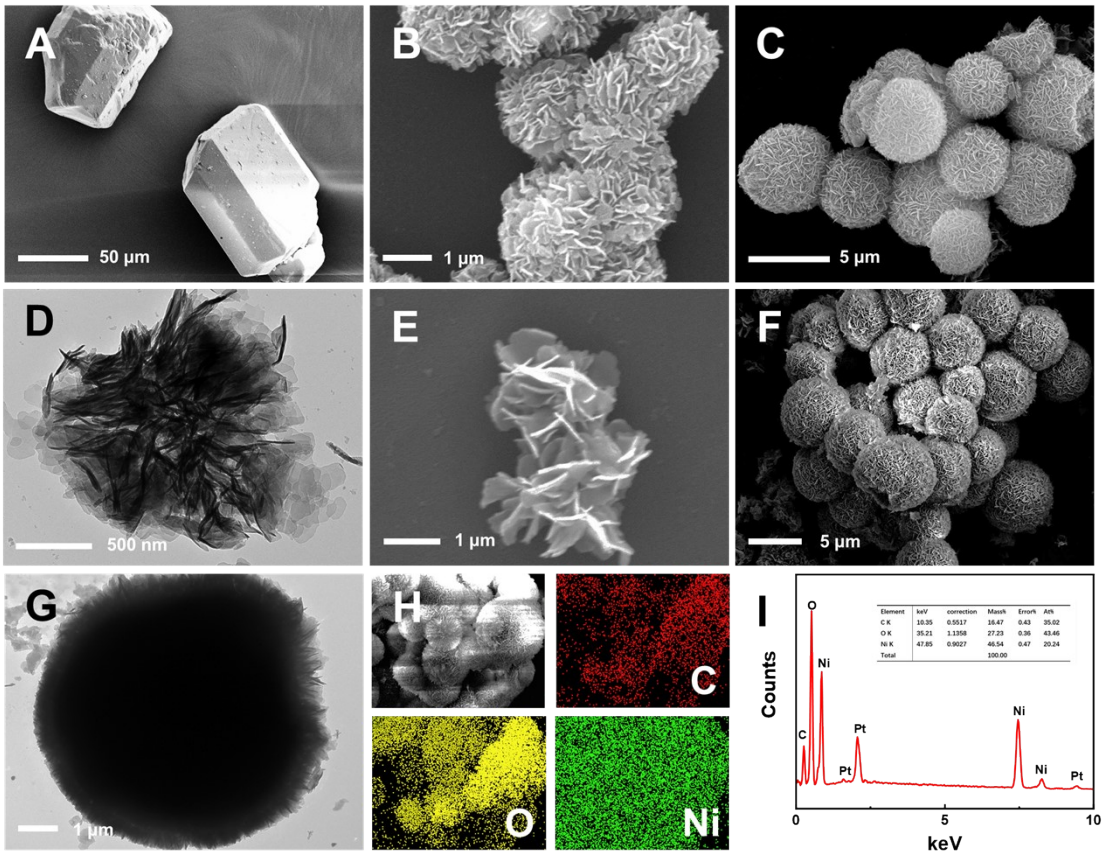

Figure S2. FE-SEM morphologies of (A) 1,2-BDC, (B) Ni-BDC (without PVP), (C) Ni-BDC. (D) TEM morphology of Ni-BDC. SEM morphologies of (E) Ni-DBP (without PVP), (F) Ni-DBP. (G) TEM morphology of Ni-DBP. (H) Elemental mapping analyses of the Ni-DBP. (I) EDS spectrogram of the Ni-DBP.

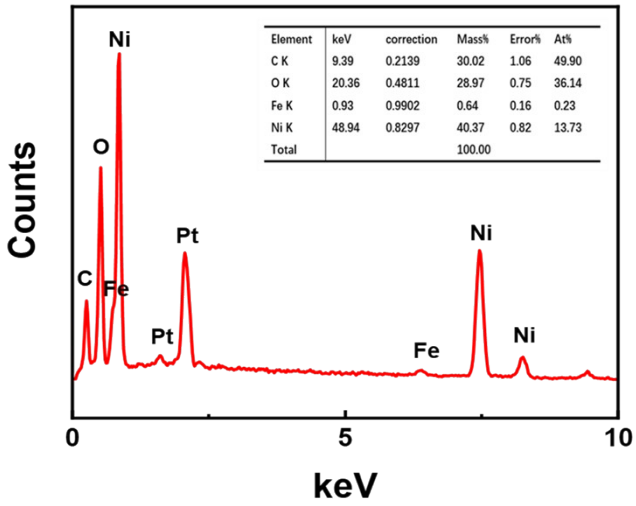

Figure S3. EDS spectrogram of the Fe_3O_4-Ni-DBP/NF.

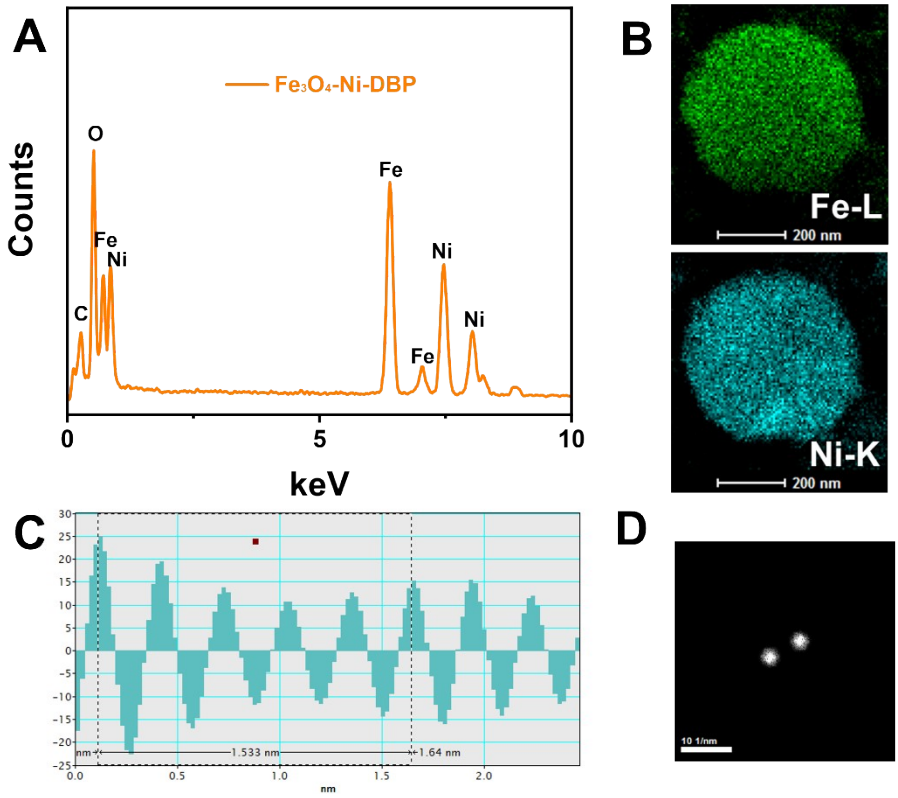

Figure S4. (A) TEM-EDS spectrogram of the Fe_3O_4-Ni-DBP. (B) Elemental mapping analyses of the Fe-L and Ni-K for Fe_3O_4-Ni-DBP. (C) Height profile and (D) topographic image of the inverse FFT mode.

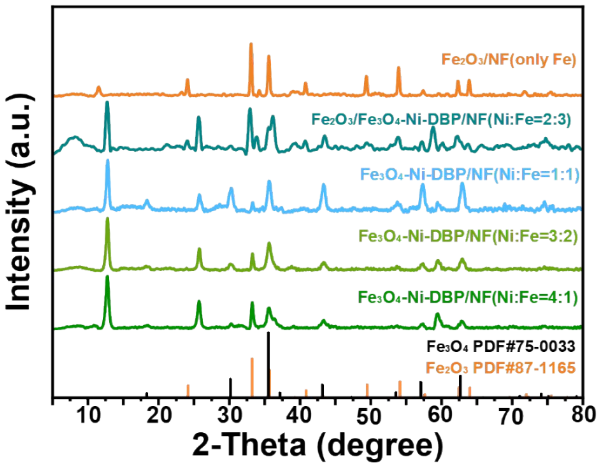

Figure S5. PXRD patterns of Fe_3O_4-Ni-DBP with different metal ratios.

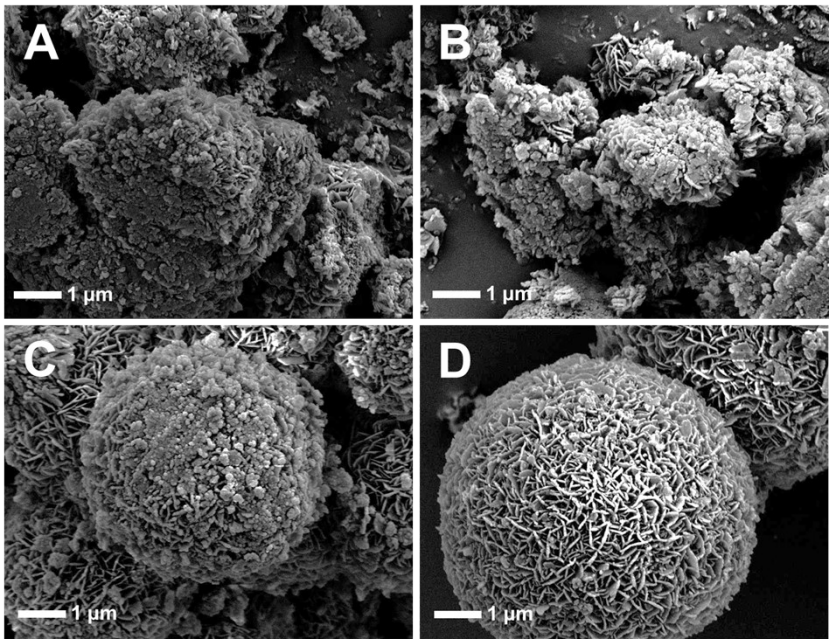

Figure S6. FE-SEM images of (A) Fe_3O_4-Ni-DBP with different metal ratios: (A) Ni:Fe = 1:4, (B) Ni:Fe = 2:3, (C) Ni:Fe = 3:2, and (D) Ni:Fe = 4:1.

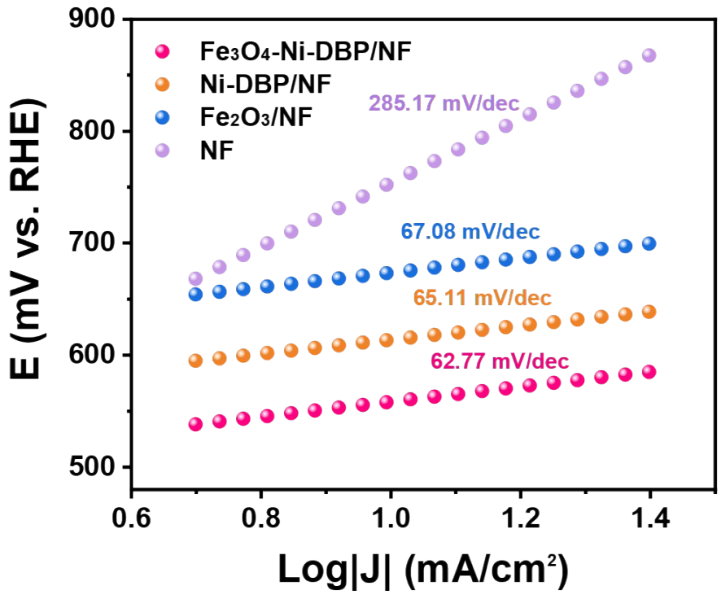

Figure S7. Tafel plot of Fe_3O_4-Ni-DBP/NF, Ni-DBP/NF, Fe_2O_3/NF, and bare NF for the OER derived from steady-state polarization measurements.

Table S1. OER performance of various electrocatalysts.

Electrocatalysts	OER η_{10} [a] (mV)	Tafel Slope (mV/dec)	Reference
Ni/FeOx NRs@CP	242	80.40	[1]
WO_3 NRs@Co-MOF/NF	280	36.00	[2]
Ni-MOF/NF-SS	253	70.90	[3]
$(Ni, Co)_2P$/NFs	283	56.40	[4]
Ni_3Se_2@NiFe-LDH/NF	222	61.30	[5]
Mo-$CoSe_2$NS@NF	234	58.00	[6]
$MoS_2/NiS_2/CoS_2$	230	89.00	[7]
Fe_3O_4-Ni-DBP/NF	**233**	**55.34**	**This work**

a: The overpotential (mV) required to drive a current density of 10 mA cm^{-2} in 1.0 M KOH.

Figure S8. CV(OER) curves of the (A) Fe_3O_4-Ni-DBP/NF, (B) Ni-DBP/NF, (C) Fe_2O_3/NF with varying scan rates (10, 20, 30, 40, 50 mV/s) in 1.0 M KOH. (D) The C_{dl} values of different catalysts.

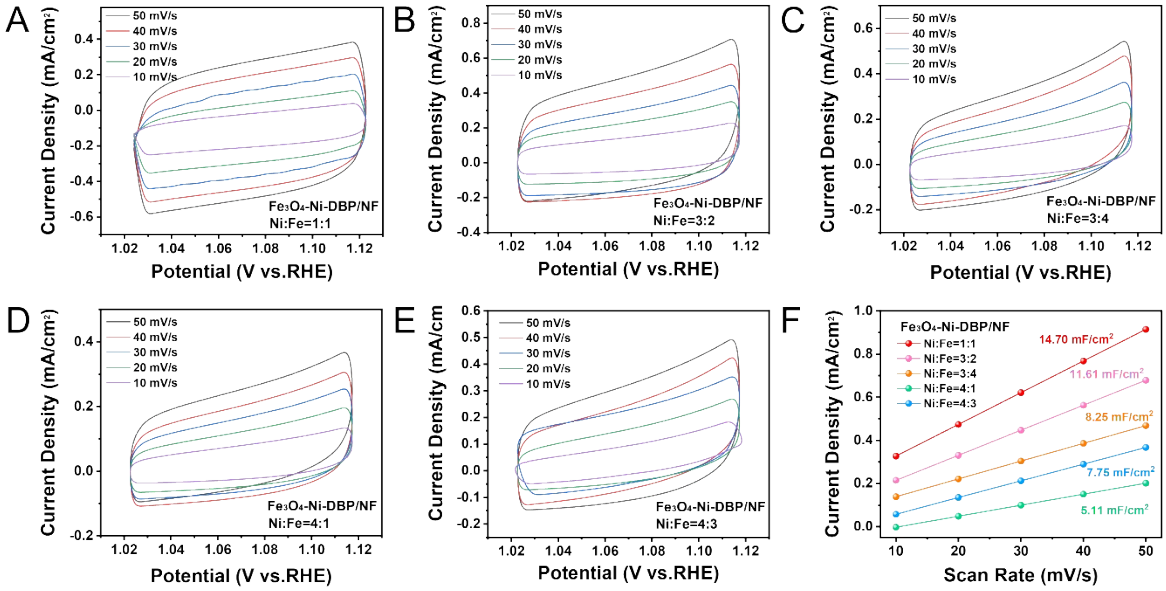

Figure S9. CV(OER) curves of the Fe_3O_4-Ni-DBP/NF with different metal ratios: (A) Ni:Fe = 1:1, (B) Ni:Fe = 3:2, (C) Ni:Fe = 3:4, (D) Ni:Fe = 4:1, (E) Ni:Fe = 4:3 with varying scan rates (10, 20, 30, 40, 50 mV/s) in 1.0 M KOH. (F) The C_{dl} values of different metal ratios.

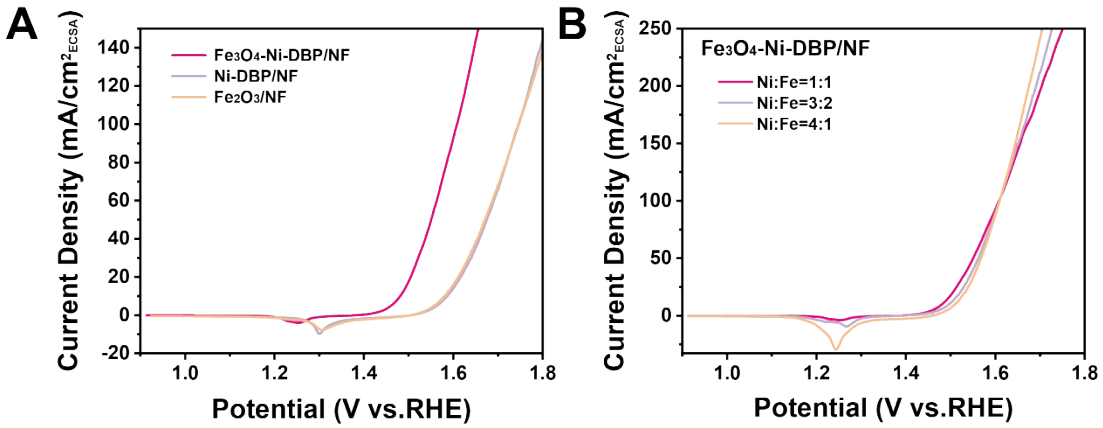

Figure S10. Normalized LSV curves based on ECSA (specific capacitance C_S = 40 μF cm^{-2}): (A) different catalysts, (B) different metal ratios.

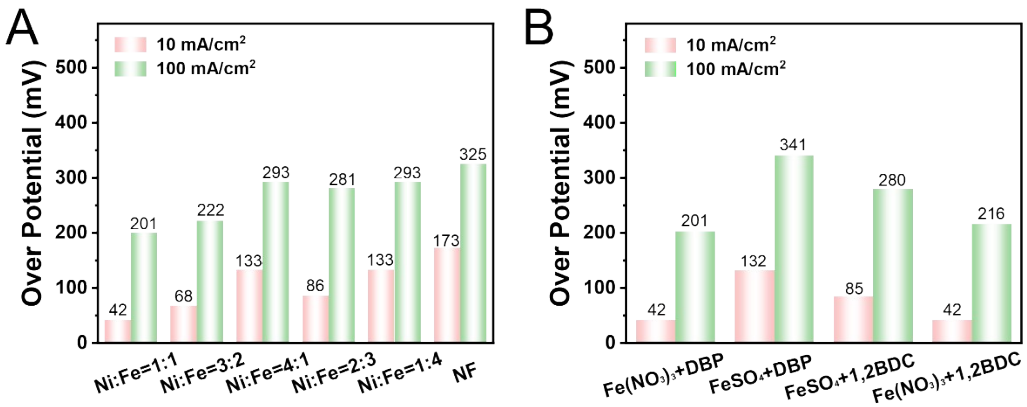

Figure S11. Overpotentials derived from HER polarization curves at 10 mA cm^{-2} and 100 mA cm^{-2}: (A) Fe_3O_4-Ni-DBP/NF with different metal ratios, (B) Fe_3O_4-Ni-DBP/NF prepared by different alternative precursors.

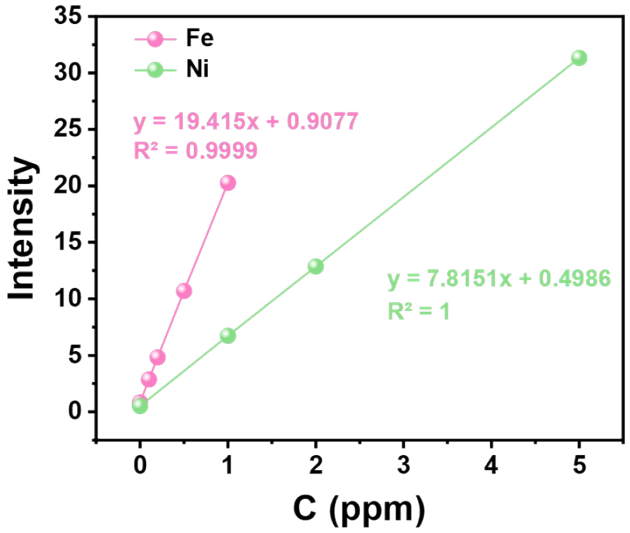

Figure S12. ICP-OES calibration curves of Fe and Ni ions.

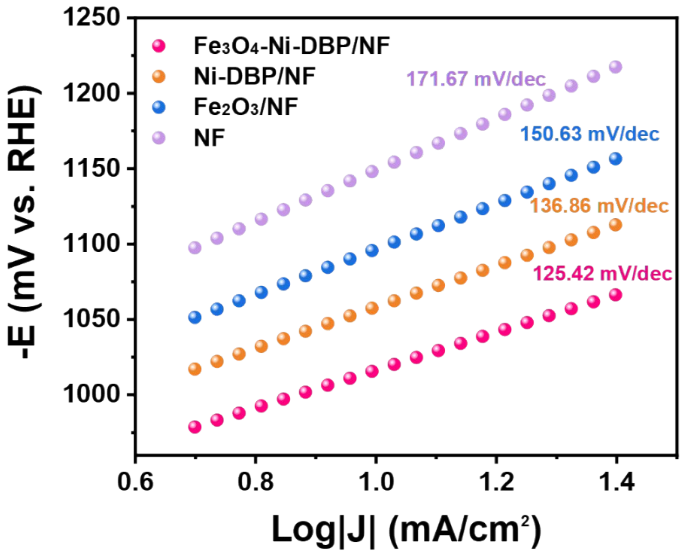

Figure S13. Tafel plot of Fe_3O_4-Ni-DBP/NF, Ni-DBP/NF, Fe_2O_3/NF, and bare NF for the HER derived from steady-state polarization measurements.

Table S2. HER performance of various electrocatalysts.

Electrocatalysts	HER η_{10} [a] (mV)	Tafel Slope (mV/dec)	Reference
Mn-MOF/NF	125	113.00	[8]
$(Ni, Co)_2P$ NFs	92	62.30	[4]
Ni_3Se_2@NiFe-LDH/NF	68	106.20	[5]
NiFe-LDH-POM/NF	156	86.00	[9]
Mo-$CoSe_2$NS@NF	89	69.00	[6]
$MoS_2/NiS_2/CoS_2$	101	116.00	[7]
Co_8FeS_8MXene/NF	108	84.08	[10]
Fe_3O_4-Ni-DBP/NF	**42**	**39.16**	**This work**

a: The overpotential (mV) required to drive a current density of 10 mA cm^{-2} in a 1.0 M KOH.

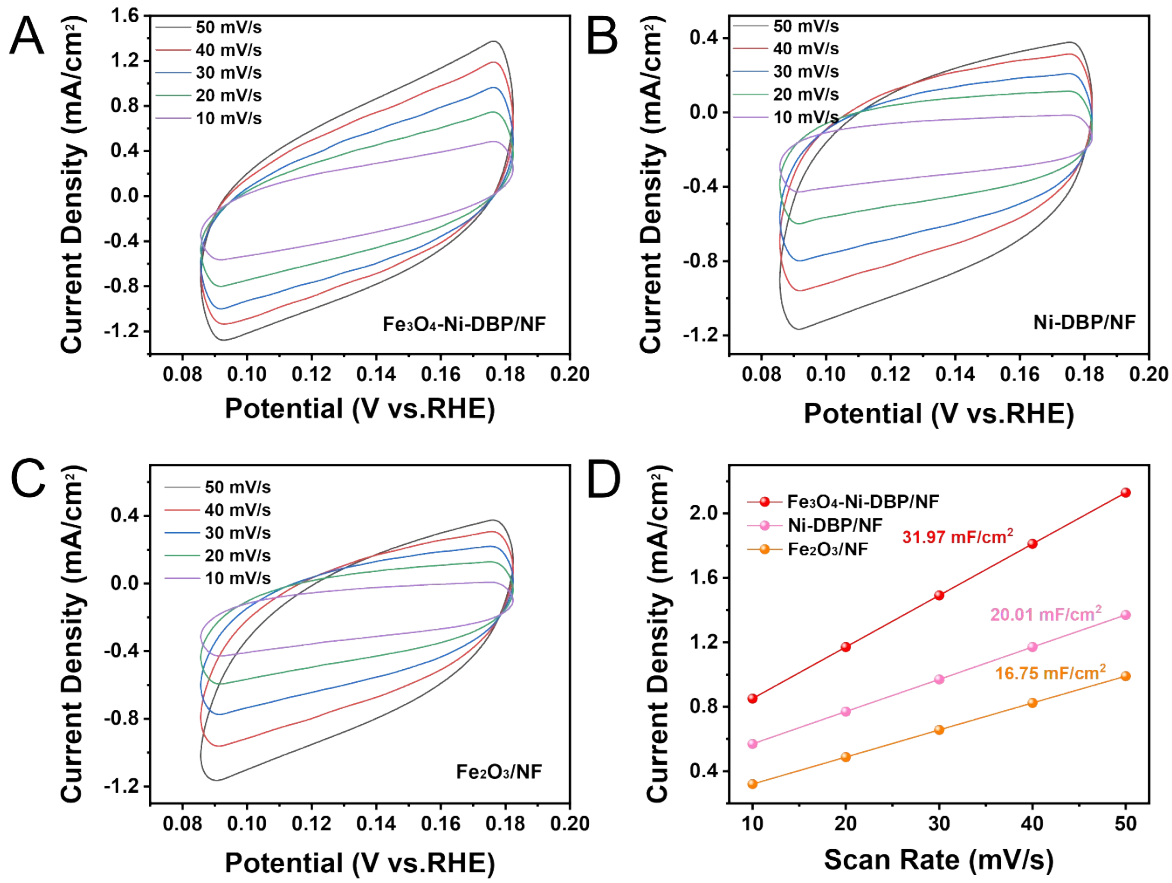

Figure S14. CV(HER) curves of the (A) Fe_3O_4-Ni-DBP/NF, (B) Ni-DBP/NF, (C) Fe_2O_3/NF with varying scan rates (10, 20, 30, 40, 50 mV/s) in 1.0 M KOH. (D) The C_{dl} values of different catalysts.

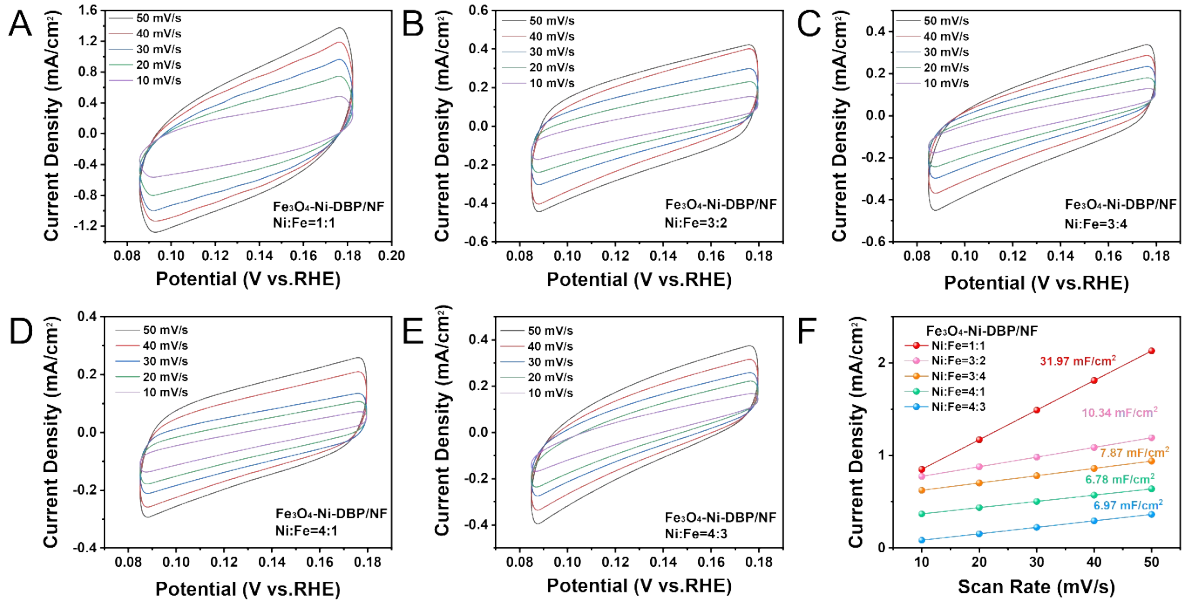

Figure S15. CV(HER) curves of the Fe_3O_4-Ni-DBP/NF with different metal ratios: (A) Ni:Fe = 1:1,

(B) Ni:Fe = 3:2, (C) Ni:Fe = 3:4, (D) Ni:Fe = 4:1, (E) Ni:Fe = 4:3 with varying scan rates (10, 20, 30, 40, 50 mV/s) in 1.0 M KOH. (F) The C_{dl} values of different metal ratios.

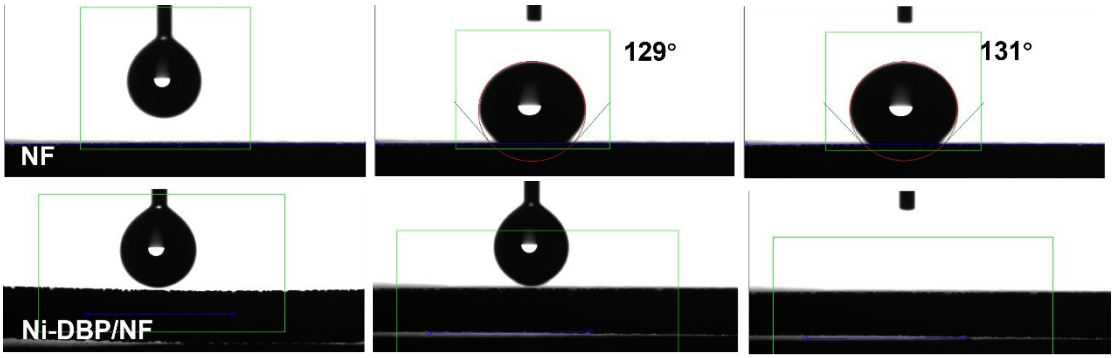

Figure S16. The static water contact angle of NF and Ni-DBP/NF.

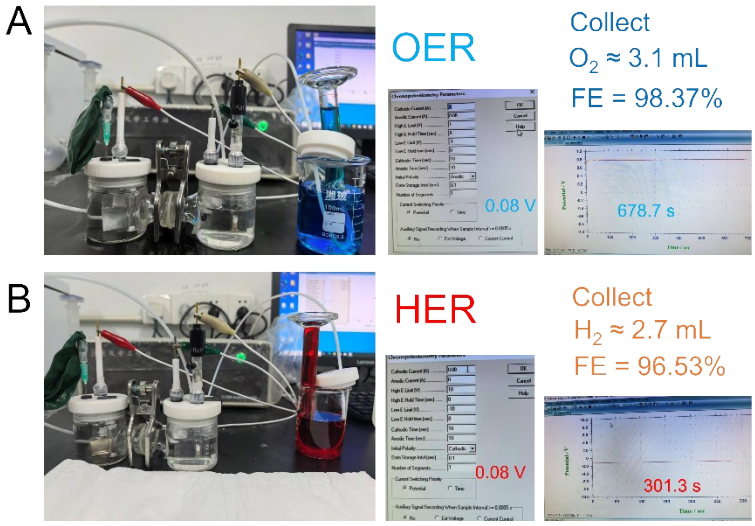

Figure S17. The O_2 (A) and H_2 (B) were collected by the water displacement method.

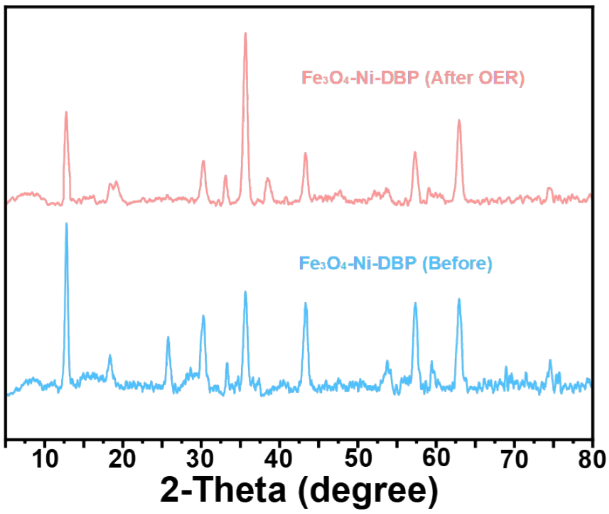

Figure S18. PXRD patterns of Fe_3O_4-Ni-DBP before and after OER in 1.0 M KOH.

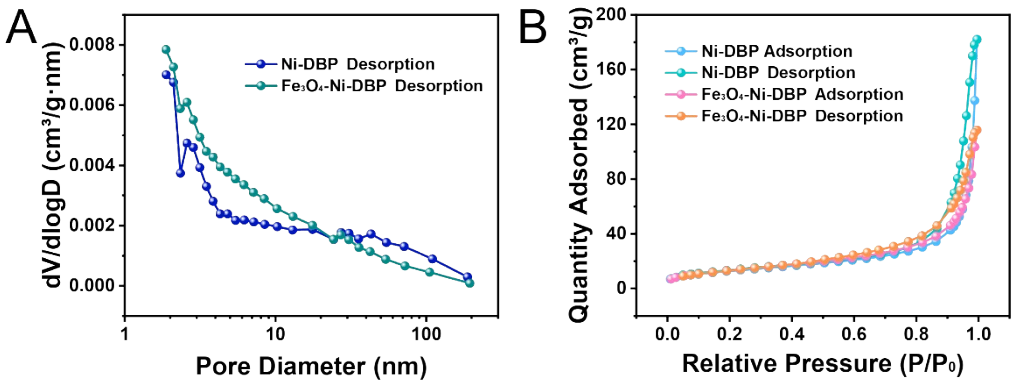

Figure S19. (A) N_2 adsorption-desorption isotherms and (B) cumulative pore-diameter distribution of pristine Ni-DBP/NF and Fe_3O_4-Ni-DBP/NF catalyst after long-term redox cycling.

Table S3 BET surface area, pore volume and average pore diameter of Ni-DBP/NF and Fe_3O_4-Ni-DBP/NF.

Samples	S_{BET} (m^2/g)	Pore volume (cm^3/g)	Average pore diameter (nm)
Ni-DBP	47.45	0.28	23.74
Fe_3O_4-Ni-DBP	49.49	0.18	13.70

Reference

1 Shaddad, M. N.; Alharthi, A. I.; Aladeemy, S. A.;Arunachalam, P., Engineering oxygen vacancy on nickel-doped iron oxide nanorods as efficient bifunctional electrocatalysts for oxygen evolution and urea oxidation reaction. *J. Taiwan Inst. Chem. E.* **2025,** *177*, 105928.

2 Wei, X.; Wang, Y.; Wang, Y.; Chai, Y.;Liu, N., Improved OER electrocatalytic performance of Co-MOF by forming heterojunction with lower-conductivity WO_3 nanorods or Cr_2O_3 nanoparticles. *Int. J. Hydrogen Energ.* **2024,** *58*, 1240-1248.

3 Wu, F.; Jiao, Y.; Ge, J.; Feng, C.; Wu, Z.; Zhu, Y.;Li, Q., Formation of Ni-MOF derived nickel sulfides as efficient electrocatalysts for oxygen evolution reaction through optimizing the sulfur sources selection. *ChemistrySelect* **2024,** *9* (37), e202403487.

4 Ji, L.; Wei, Y.; Wu, P.; Xu, M.; Wang, T.; Wang, S.; Liang, Q.; Meyer, T. J.;Chen, Z., Heterointerface engineering of Ni_2P-Co_2P nanoframes for efficient water splitting. *Chem. Mater.* **2021,** *33* (23), 9165-9173.

5 Hu, J.; Zhu, S.; Liang, Y.; Wu, S.; Li, Z.; Luo, S.;Cui, Z., Self-supported Ni_3Se_2@NiFe layered double hydroxide bifunctional electrocatalyst for overall water splitting. *J. Colloid. Interf. Sci.* **2021,** *587*, 79-89.

6 Huang, J.; Wang, S.; Nie, J.; Huang, C.; Zhang, X.; Wang, B.; Tang, J.; Du, C.; Liu, Z.;Chen, J., Active site and intermediate modulation of 3D $CoSe_2$ nanosheet array on Ni foam by Mo doping for high-efficiency overall water splitting in alkaline media. *Chem. Eng. J.* **2021,** *417*, 128055.

7 Yin, Z.; Liu, X.; Chen, S.; Xie, H.; Gao, L.; Liu, A.; Ma, T.;Li, Y., Interface engineering of the MoS_2/NiS_2/CoS_2 nanotube as a highly efficient bifunctional electrocatalyst for overall water splitting. *Mater. Today Nano* **2022,** *17*, 100156.

8 Goswami, A.; Ghosh, D.; Pradhan, D.; Biradha, K., In situ grown Mn(II) MOF upon nickel foam acts as a robust self-supporting bifunctional electrode for overall water splitting: A bimetallic synergistic collaboration strategy. *ACS Appl. Mater. Interfaces* **2022,** *14* (26), 29722-29734.

9 Li, C.; Zhang, Z.;Liu, R., In situ growth of 3D NiFe LDH-POM micro-flowers on nickel foam for overall water splitting. *Small* **2020,** *16* (46), 2003777.

10 Gong, Z.; Dai, Z.; Dong, Z.; Liu, Q.; Milichko, V. A.; Liu, H.; Liu, J.; Niu, R.;Gong, J., Green synthesis of luminescent La-MOF nanoparticle from waste poly(ethylene terephthalate) for high-

performance in Fe(III) detection. *Rare Met.* **2024,** *43* (8), 3833-3843.